Electronic Supplementary Information

Novel Pyridine-Based Thiazolyl-Hydrazone as a Promising Attenuator of *Pseudomonas aeruginosa* Pathogenicity by Targeting Quorum Sensing

Anabela Borges [1,2,*,†], Sanja Kokanov [3,†], Miguel M. Leitão [1,4], Predrag Ristić [3], Irena Novaković [5], Vladimir Dobričić [6], Milan Nikolić [3], Mire Zloh [7,8], Tamara R. Todorović [3], Manuel Simões [1,2] and Nenad R. Filipović [9,*]

[1] LEPABE (Laboratory for Process Engineering, Environment, Biotechnology and Energy, Faculty of Engineering), ALiCE (Associate Laboratory for Innovation in Chemical Engineering), Faculty of Engineering, University of Porto, Rua Dr. Roberto Frias, s/n, 4200-465 Porto, Portugal; up202111359@edu.fe.up.pt (M.M.L.); mvs@fe.up.pt (M.S.)
[2] DEQB—Department of Chemical and Biological Engineering, Faculty of Engineering, University of Porto, Rua Dr. Roberto Frias, s/n, 4200-465 Porto, Portugal
[3] Faculty of Chemistry, University of Belgrade, Studentski trg 12-16, 11000 Belgrade, Serbia; markovics@chem.bg.ac.rs (S.K.); predrag@chem.bg.ac.rs (P.R.); mnikolic@chem.bg.ac.rs (M.N.); tamarat@chem.bg.ac.rs (T.R.T.)
[4] MedInUP, Center for Drug Discovery and Innovative Medicines, University of Porto, 4200-319Porto, Portugal
[5] Institute of Chemistry, Technology and Metallurgy, University of Belgrade, Njegoševa 12, 11000 Belgrade, Serbia; irena.novakovic @ihtm.bg.ac.rs
[6] Department of Pharmaceutical Chemistry, Faculty of Pharmacy, University of Belgrade, Vojvode Stepe 450, 11221 Belgrade, Serbia; vladimir@pharmacy.bg.ac.rs
[7] UCL School of Pharmacy, University College London, 29/39 Brunswick Square, London WC1N 1AX, UK; mire.zloh@ffns.ac.rs
[8] Faculty of Pharmacy Novi Sad, University Business Academy in Novi Sad, Heroja Pinkija 4, 21101 Novi Sad, Serbia
[9] Faculty of Agriculture, University of Belgrade, Nemanjina 6, 11000 Belgrade, Serbia
* Correspondence: apborges@fe.up.pt (A.B.); nenadf@agrif.bg.ac.rs (N.R.F.); Tel.: +351-22041-4968 (A.B.); +381-11441-3148 (N.R.F.)
† These authors contributed equally to this manuscript.

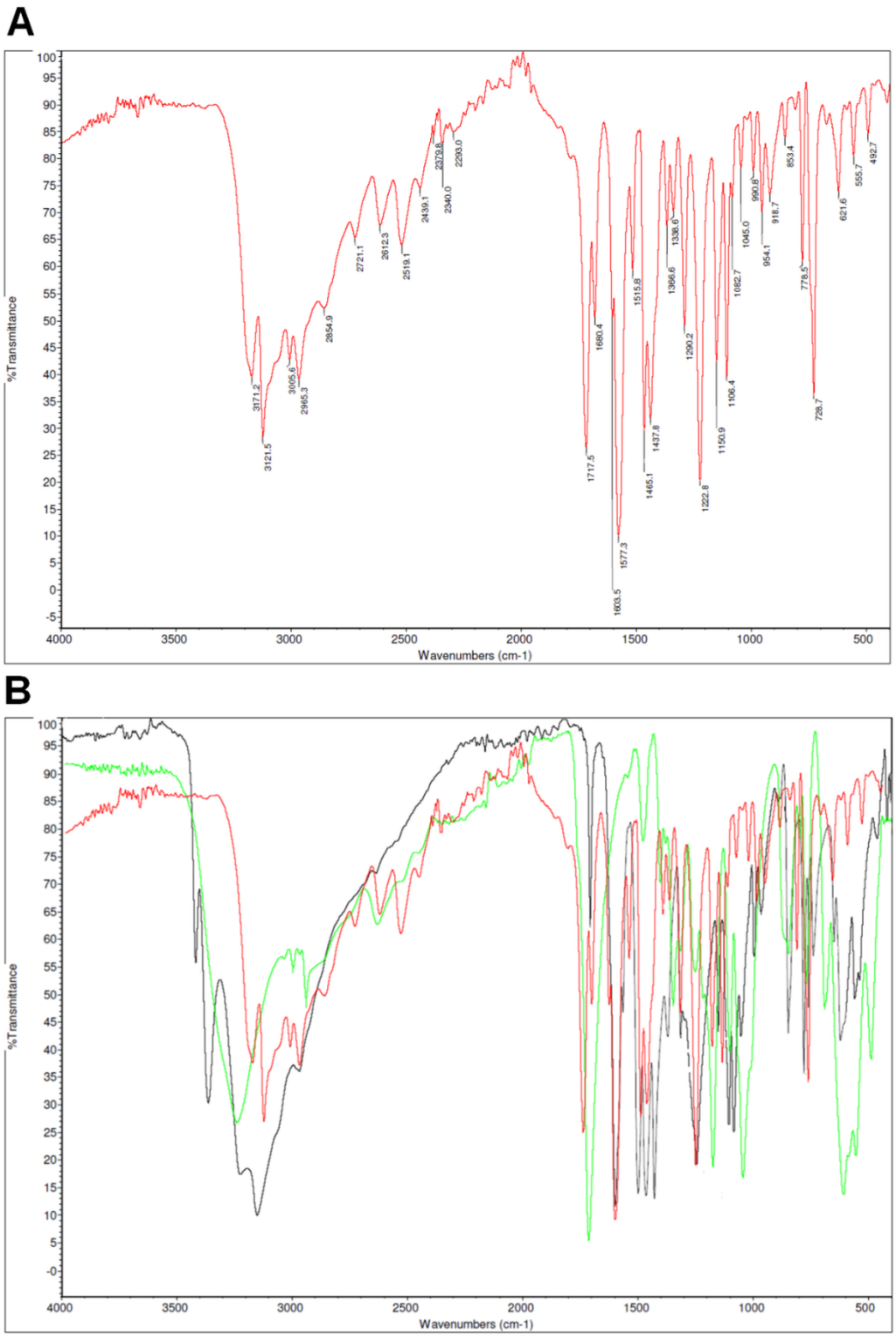


Figure S1. A) FTIR spectrum of **TTNF37,** B) Overlay of the FTIR spectra of the reactants 2-acetylpyridine thiosemicarbazone (black line) and bromopyruvic acid (green line) with the product **TTNF37** (red line).

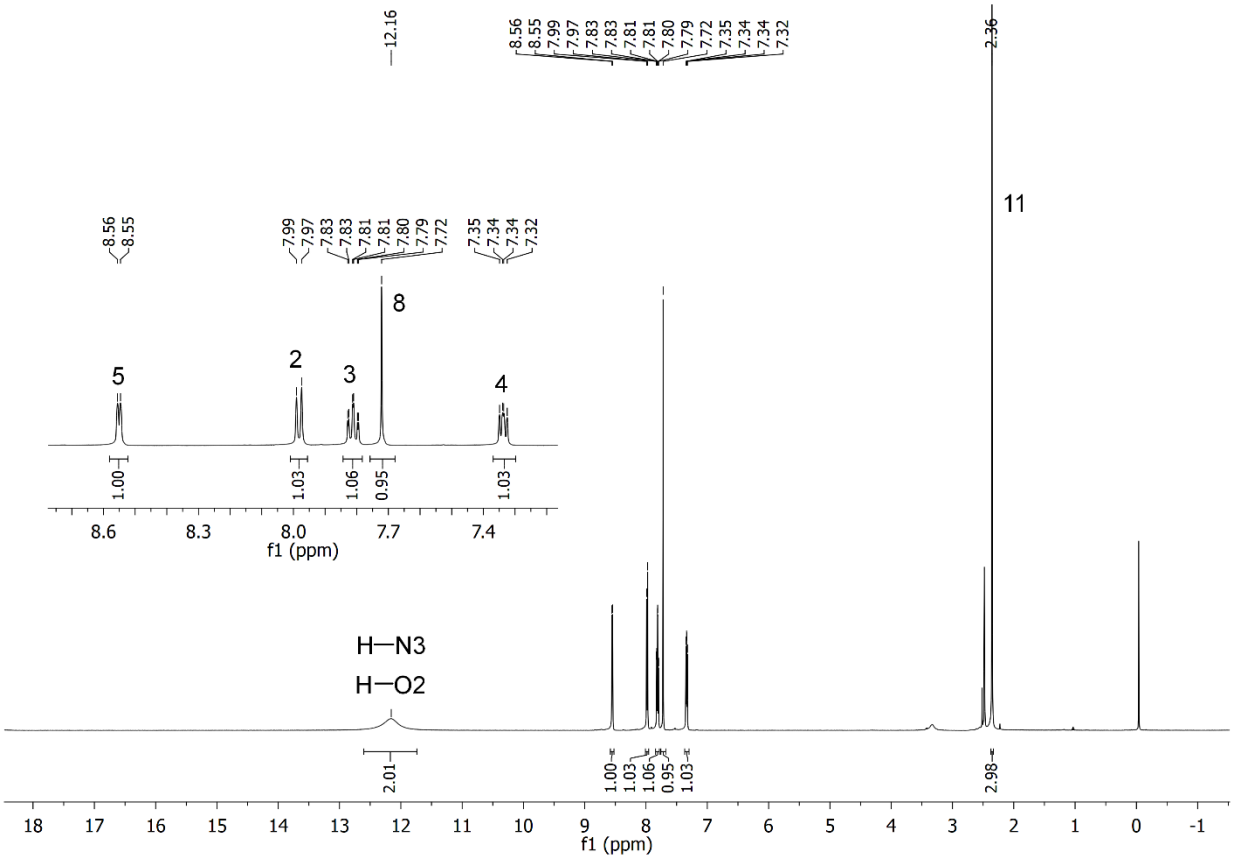


Figure S2. ^{1}H NMR spectrum of **TTNF37** in DMSO-d_6.

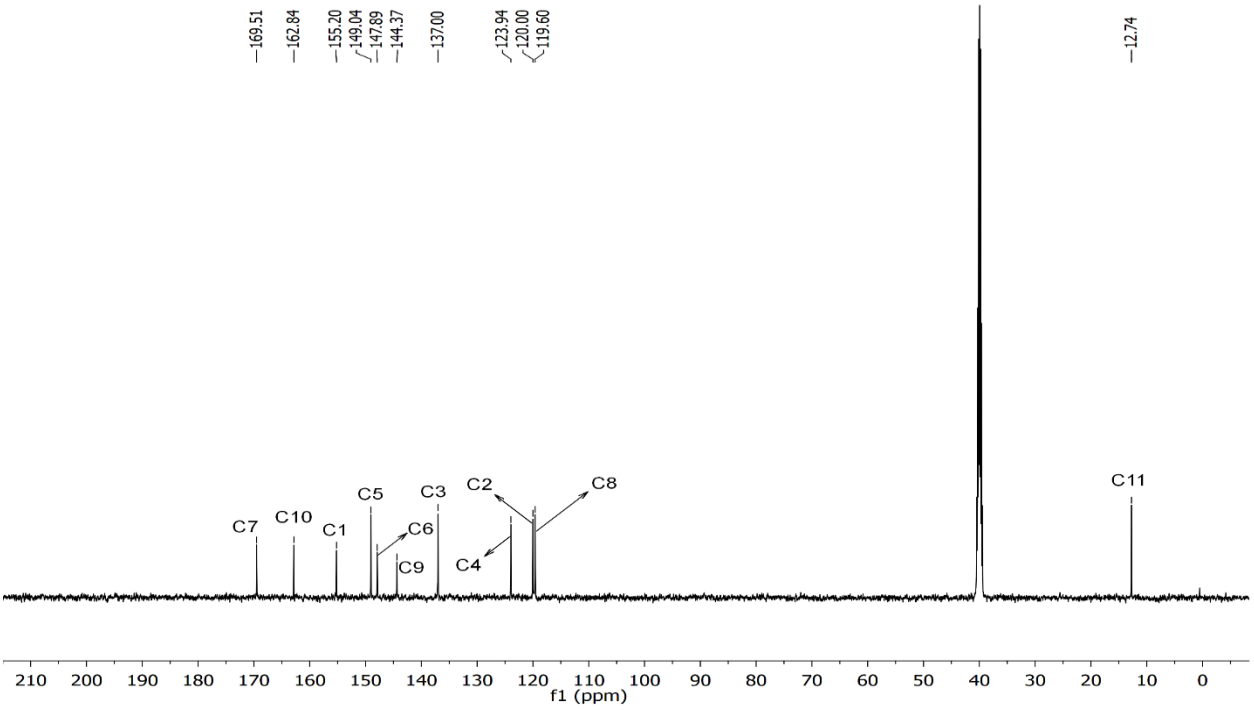


Figure S3. ^{13}C NMR spectrum of **TTNF37** in DMSO-d_6.

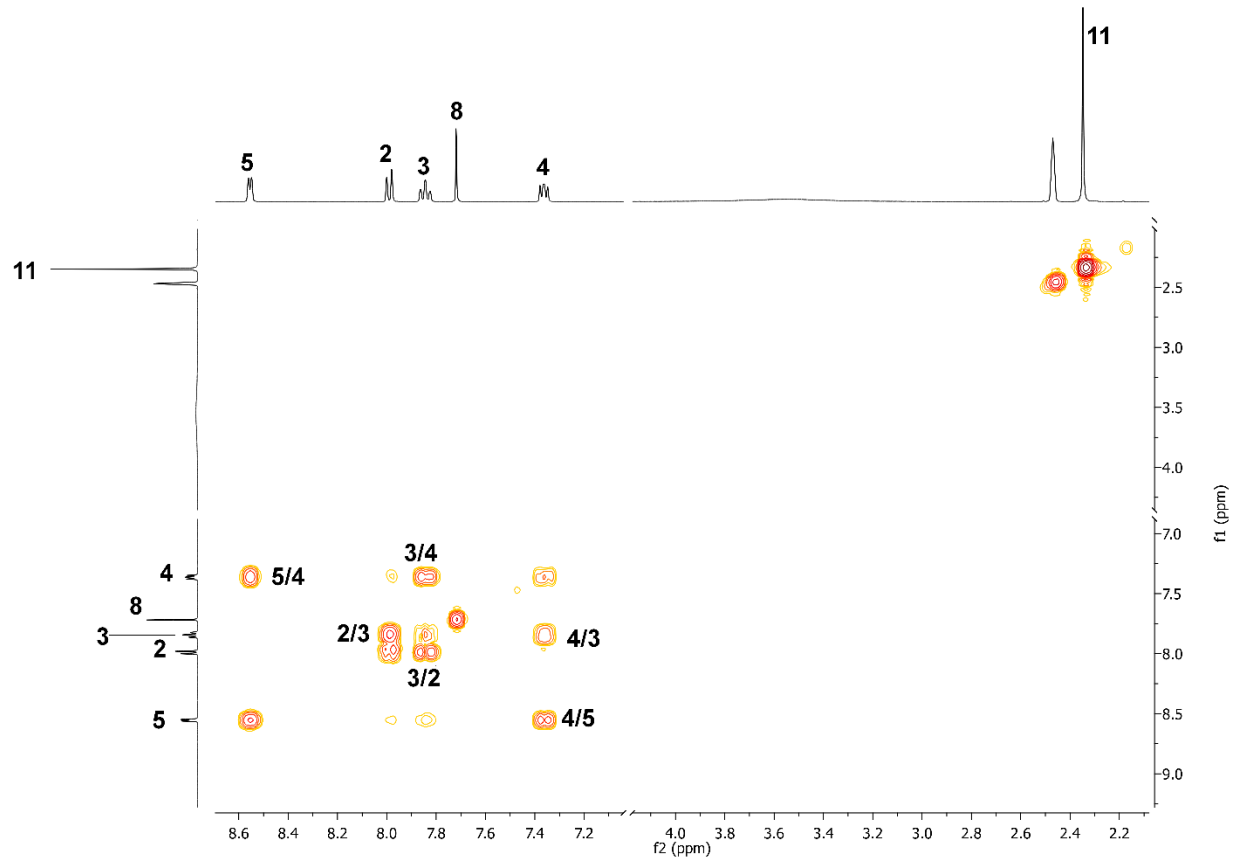


Figure S4. COSY spectrum of **TTNF37** in DMSO-*d*6

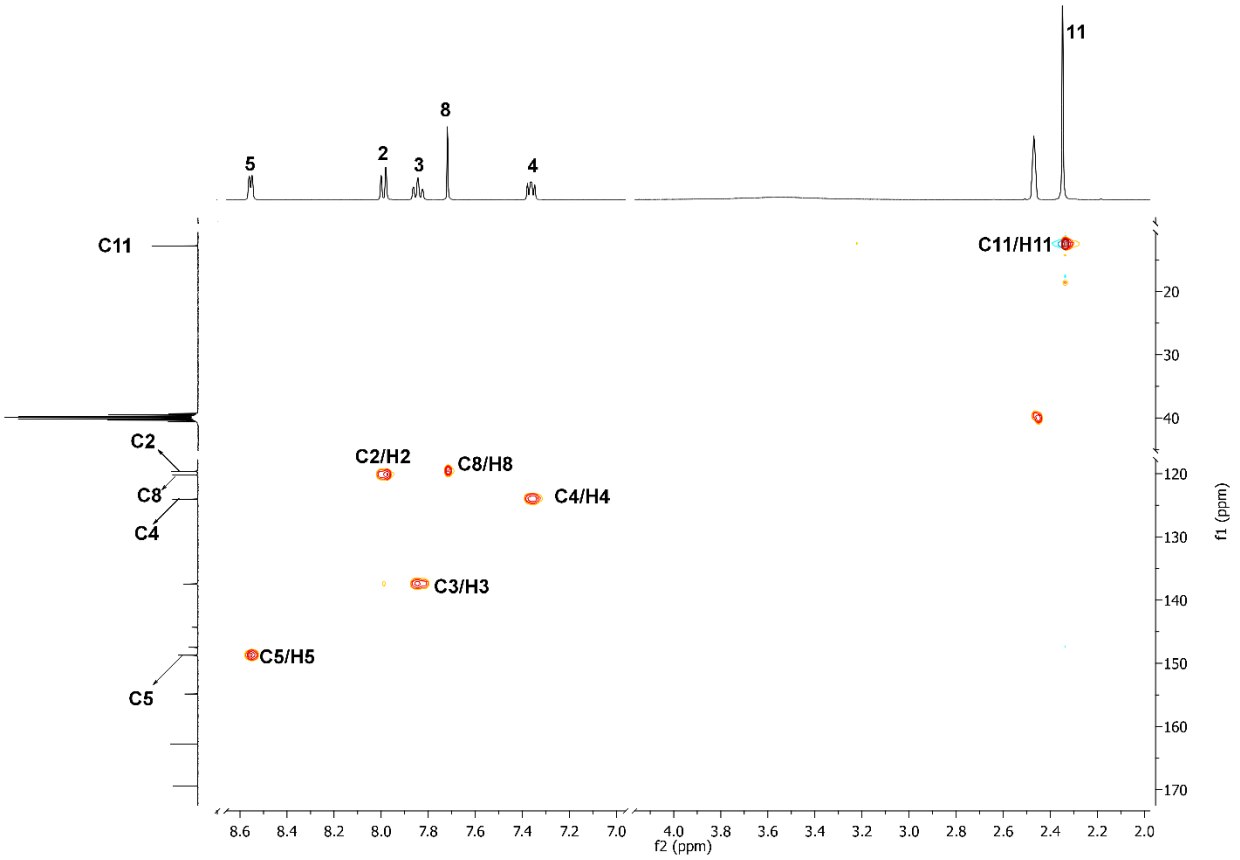


Figure S5. ^{1}H-^{13}C HSQC spectrum of **TTNF37** in DMSO-*d*6

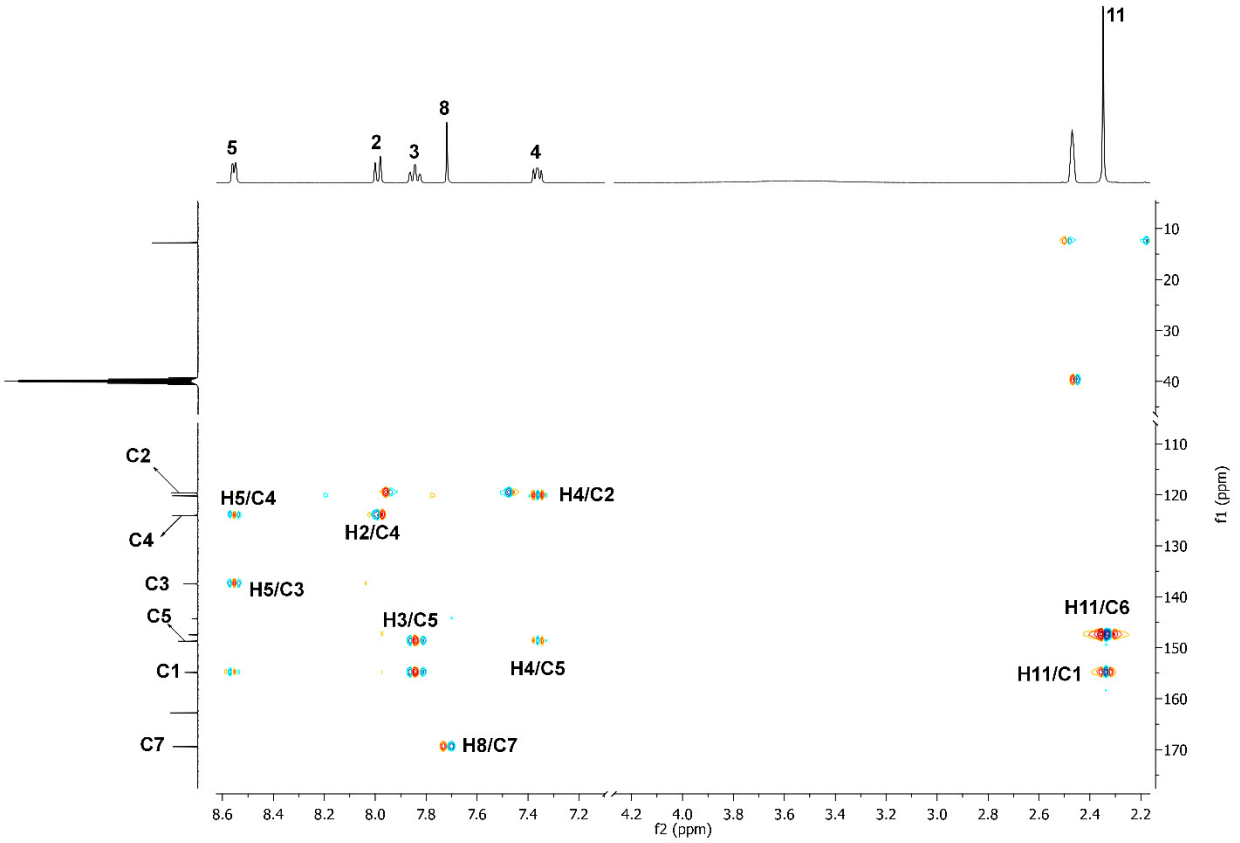


Figure S6. ^{1}H-^{13}C HMBC spectrum of **TTNF37** in DMSO-*d*6

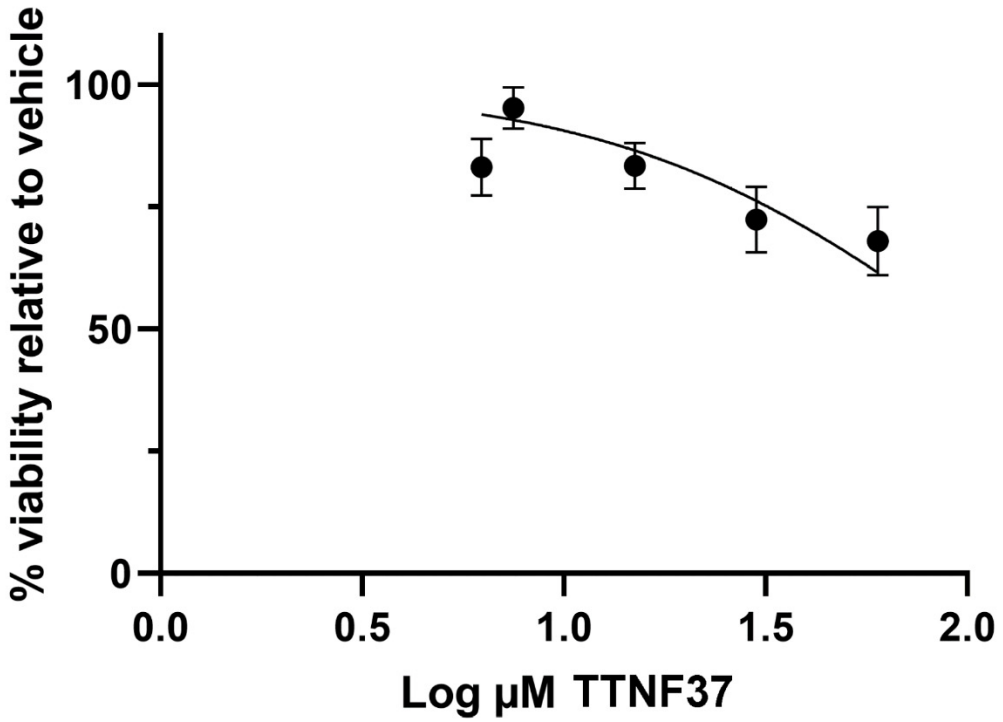


Figure S7. Effect of increasing concentrations of **TTNF37** on % cell viability compared to vehicle.

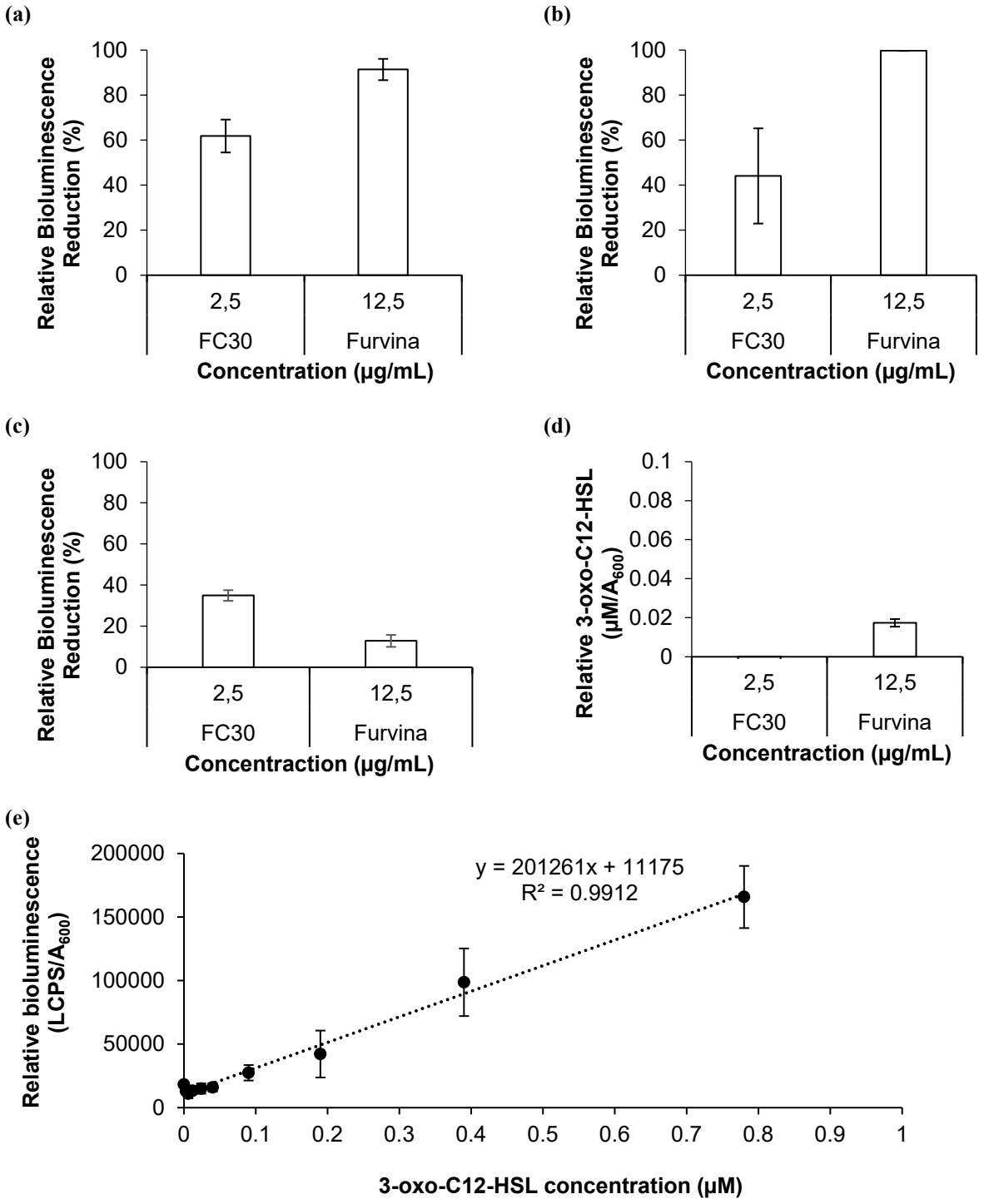


Figure S8. Positive controls with furanone C-30 (FC30) (known QS inhibitor) at 2.5 µg/mL and Furvina (known *P. aeruginosa* LasI/R QS inhibitor) at 12.5 µg/mL. Interference of FC30 and Furvina with *P. aeruginosa* 3-oxo-C12-HSL-based QS system (a). Effect of FC30 and Furvina on both 3-oxo-C12-HSL detection by PA14-R3 (b) and 3-oxo-C12-HSL production by PA14 wild-type (c). The concentration of 3-oxo-C12-HSL present in culture supernatant of

PA14 wild-type strain previously exposed to FC30 (2.5 µg/mL) and Furvina (12.5 µg/mL) was detected by PA14-R3 biosensor and quantitatively determined (d) based on an equation derived from the calibration curve (e). Mean values ± standard deviations for at least three replicates are illustrated.

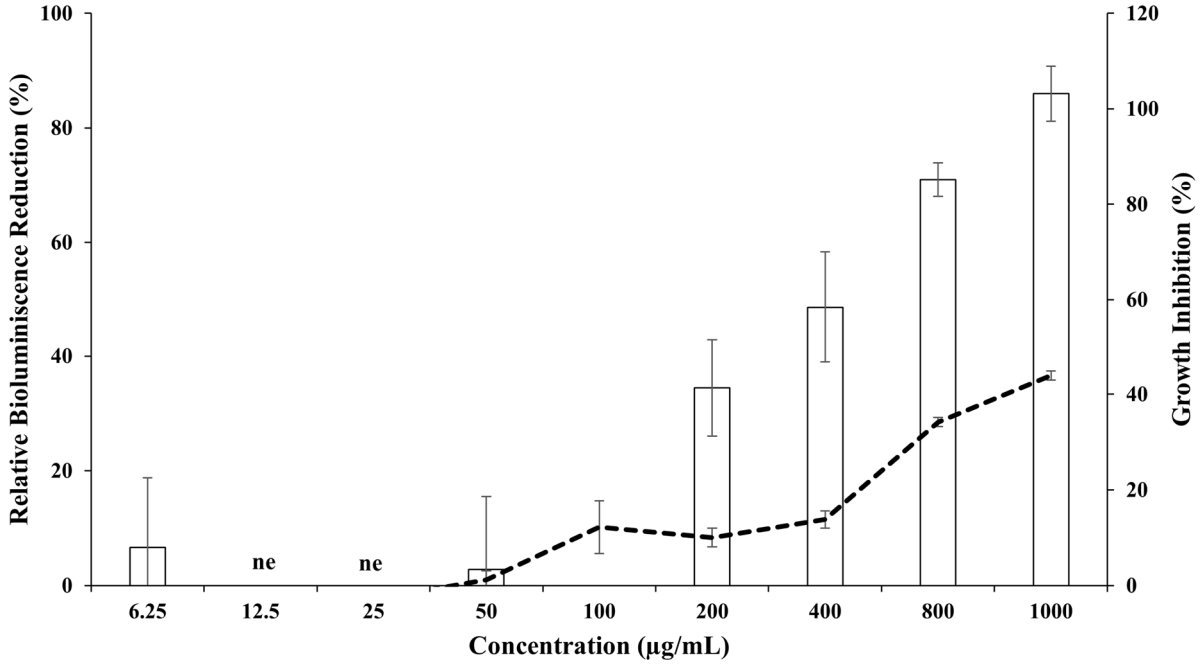


Figure S9. Effect of increasing concentrations of **TTNF37** (6.25 to 1000 µg/mL) on *P. aeruginosa* 3-oxo-C12-HSL-dependent QS system and on growth inhibition after 24 h of incubation. Bioluminescence emissions were normalized to the cell density of the bacterial culture and expressed as percentages with respect to untreated controls (relative bioluminescence). ne = no effect. Mean values ± standard deviations for at least three replicates are illustrated.

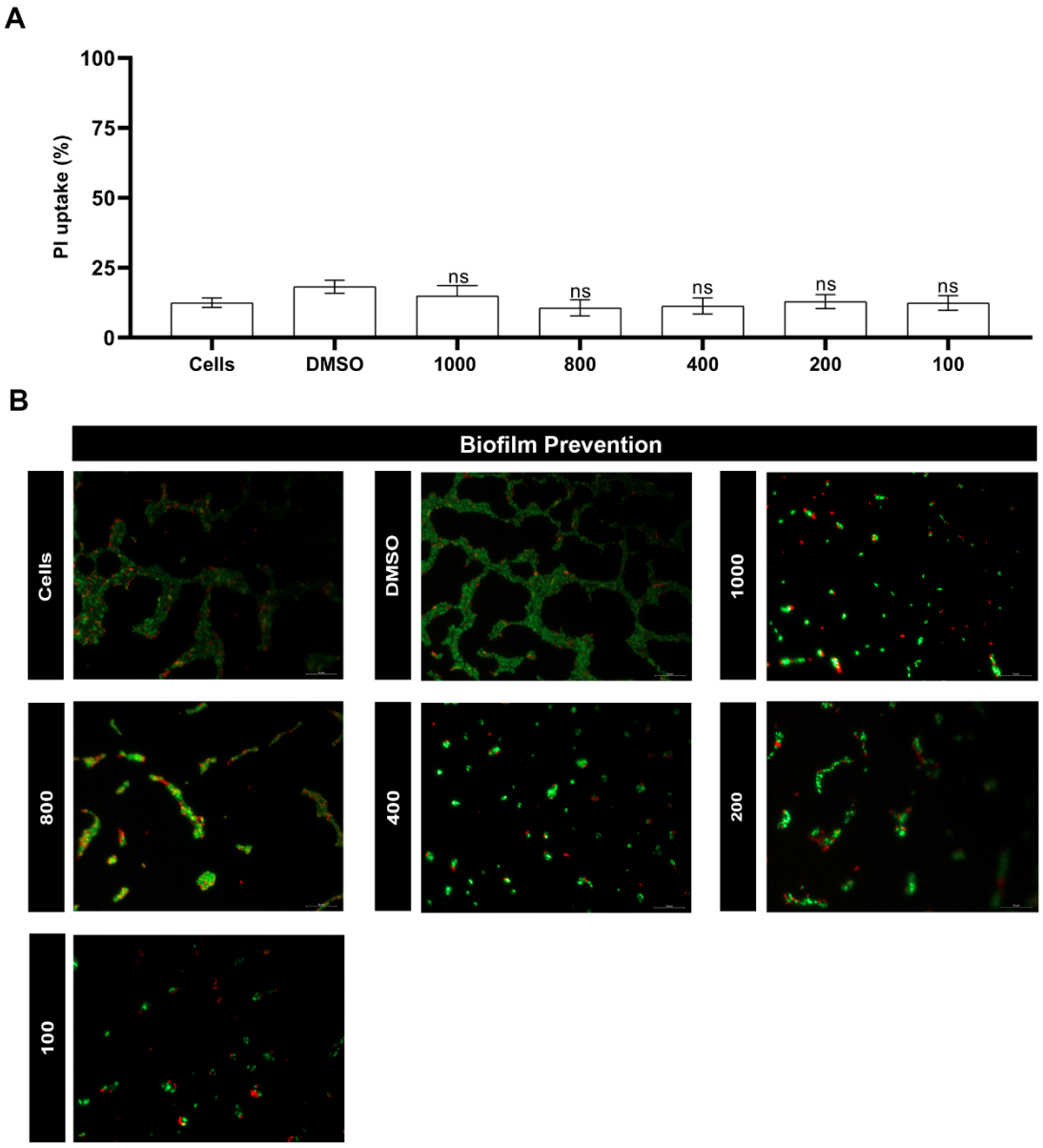


Figure S10. Effect of **TTNF37** (at 1000, 800, 400, 200, and 100 µg mL^{-1}) against PA14-WT biofilms in terms of membrane integrity evaluated by flow cytometry (**A**) and epifluorescence microscopy (**B**) using PI and live/death kit, respectively (the scale bar corresponds to 10 µm). Mean values ± standard deviations for at least three replicates are shown. Bars marked with "*" indicate statistical significance compared to the negative control (cells or DMSO) at a confidence level greater than 95 % ($p < 0.05$); ns= non- significant.

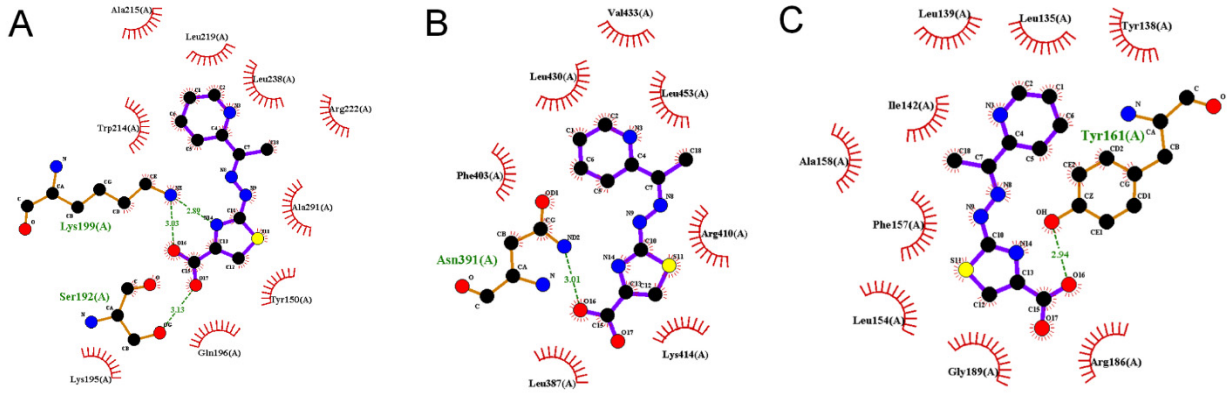


Figure S11. Schematic drawings of the interactions of the first GOLD cluster-docked solutions of **monoanionic TTNF37**@ Sudlow's site I (**A**), Sudlow's site II (**B**), and Drug binding site 3 (**C**) (PDB IDs: 2BXD, 2BXG, and 1BJ5, respectively) generated using LIGPLUS. Dashed lines are hydrogen bonds and 'eyelashes' show residues involved in hydrophobic interactions.

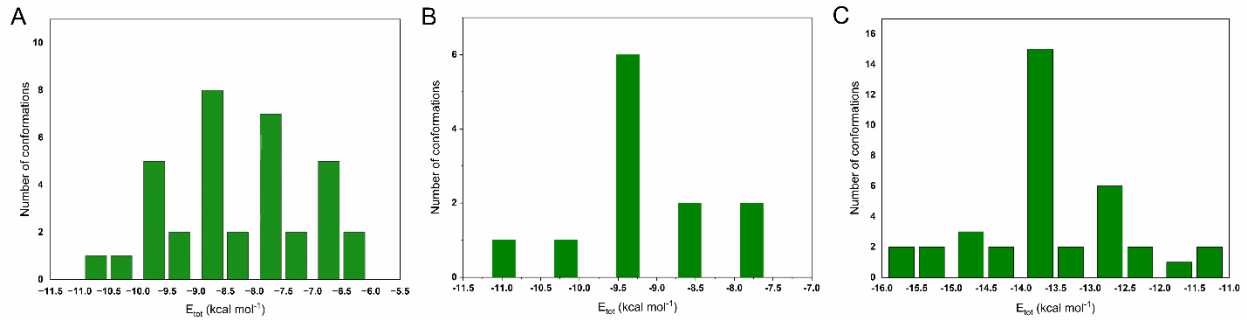


Figure S12. Cluster analysis of docking results of **monoanionic TTNF37**@ Sudlow's site I (**A**), Sudlow's site II (**B**), and Drug binding site 3 (C) (PDB IDs: 2BXD, 2BXG, and 1BJ5, respectively) using a 1.0 Å RMSD cluster tolerance.

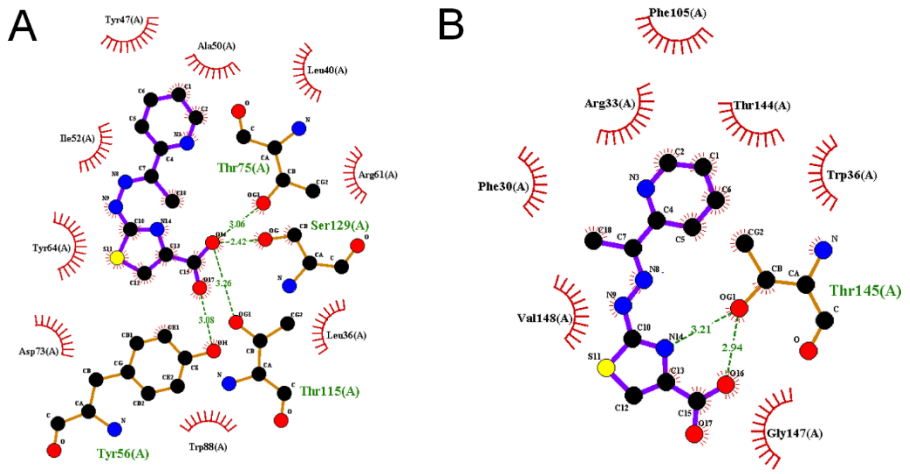


Figure S13. Schematic drawings of the interactions of the first GOLD cluster docked solutions of **monoanionic TTNF37**@LasR transcriptional activator (PDB ID: 3IX3, **A**) and AHL Synthase LasI (PDB ID: 1RO5, **B**)

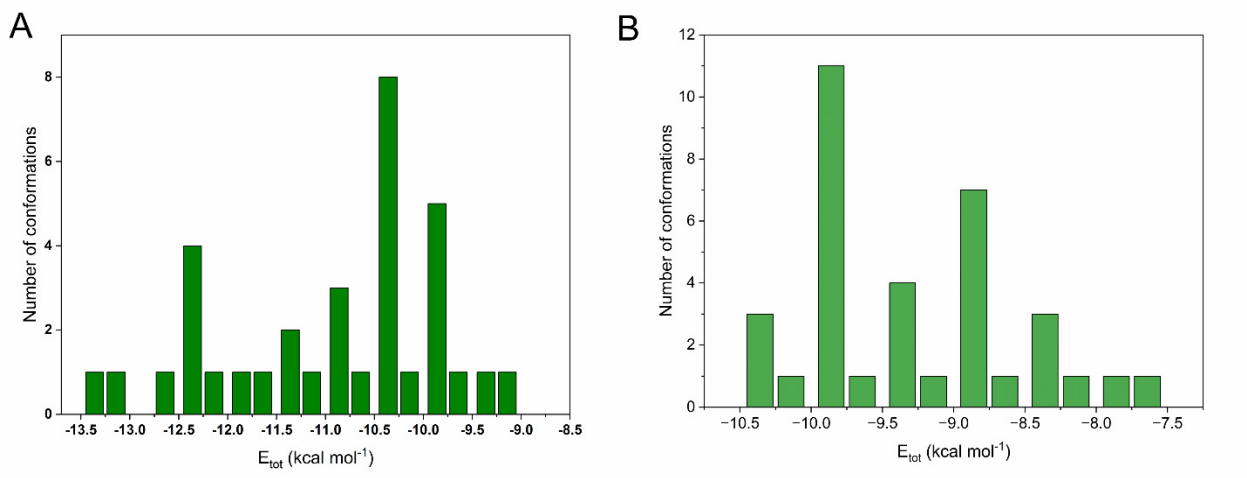


Figure S14. Cluster analysis of docking results of **monoanionic TTNF37**@ LasR transcriptional activator (PDB ID: 3IX3, **A**) and AHL Synthase LasI (PDB ID: 1RO5, **B**) using a 1.0 Å RMSD cluster tolerance.

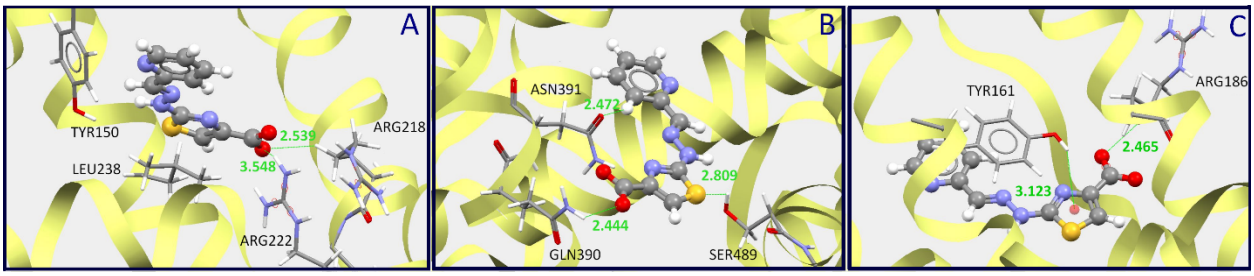


Figure S15. Three-dimensional bioactive conformations of monoanionic **1** in Sudlow site 1 (**A**), Sudlow site 2 (**B**), and Drug binding site 3 (C) are shown in ball and stick representation, with the corresponding molecular environment in the cavity. Amino acids that interact with ligands by non-covalent interactions (green lines) are shown in capped sticks style with a three-letter code and a sequence number in the protein sequence. Amino acids and ligand atoms are represented by standardized CCDC colors (the gray color represents the 1 carbon core, the red color represents the oxygen atoms, the bluish-purple color represents the nitrogen atom, and the white color represents the hydrogen atoms). The complete amino acid environment in the binding pocket is illustrated in the 2D plots generated using LIGPLUS [71]; however, it is omitted here for clarity.

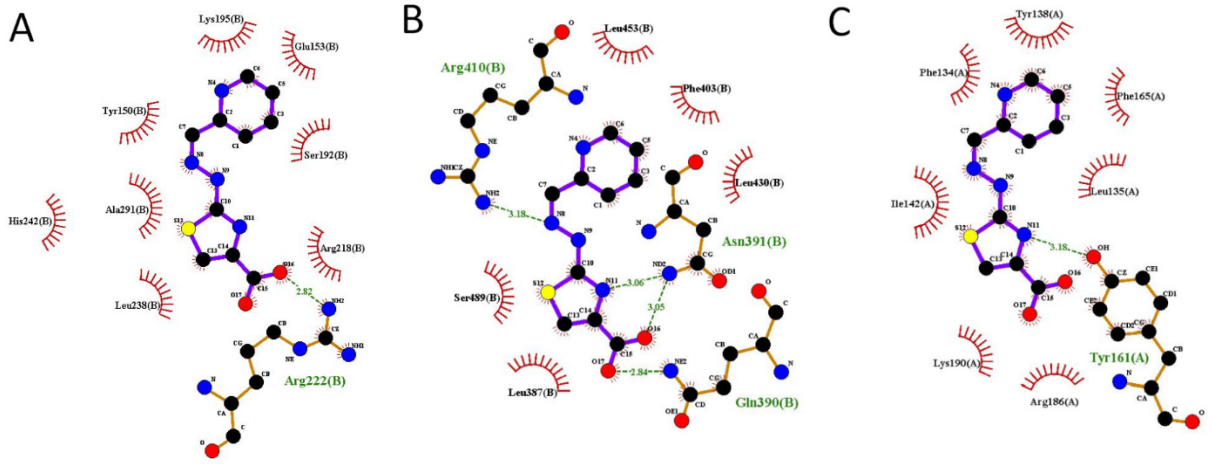


Figure S16. Schematic drawings of the interactions of the first GOLD cluster-docked solutions of **monoanionic 1**@ Sudlow's site I (**A**), Sudlow's site II (**B**), and Drug binding site 3 (**C**) (PDB IDs: 2BXD, 2BXG, and 1BJ5, respectively) generated using LIGPLUS. Dashed lines are hydrogen bonds, and 'eyelashes' show residues involved in hydrophobic interactions.

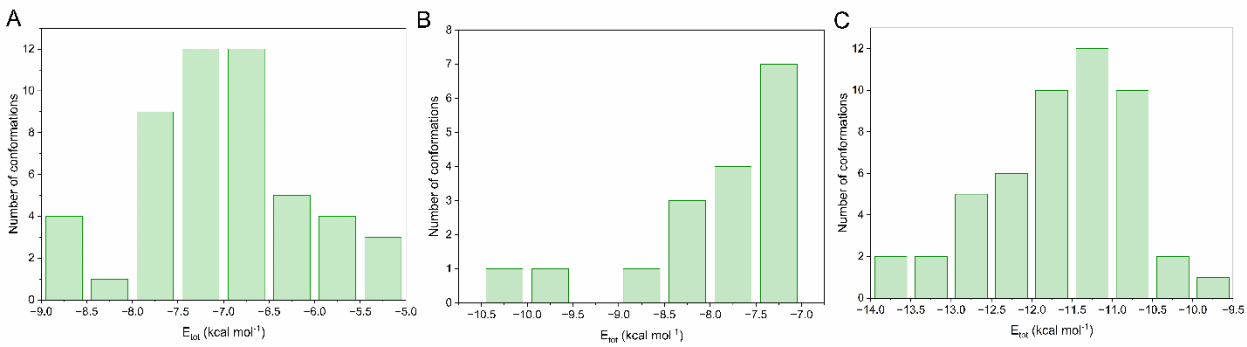


Figure S17. Cluster analysis of docking results of **monoanionic 1**@ Sudlow's site I (**A**), Sudlow's site II (**B**), and Drug binding site 3 (C) (PDB IDs: 2BXD, 2BXG, and 1BJ5, respectively) using a 1.0 Å RMSD cluster tolerance.

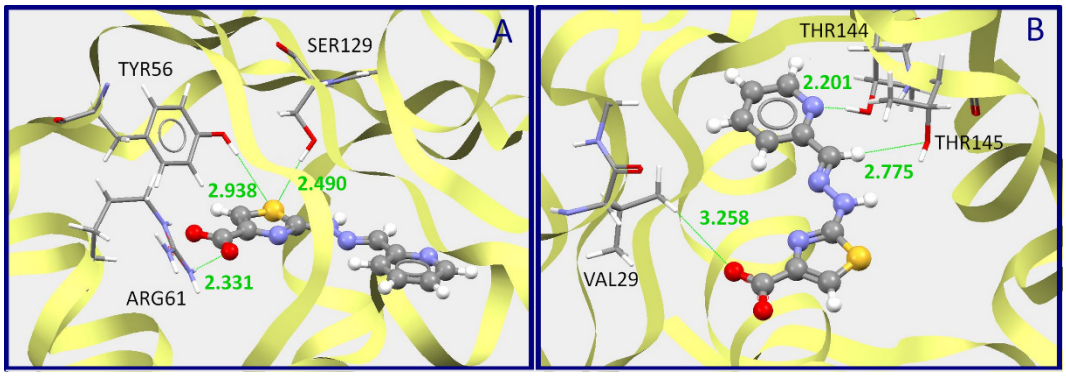


Figure S18. Three-dimensional bioactive conformations of monoanionic **1** canonical site of LasR (PDB ID: 3IX3; **A**) and LasI-AHL synthase (PDB ID: 1RO5; **B**) are shown in ball-and-stick representation, with corresponding molecular environment in the cavity. Amino acids that interact with ligands by non-covalent interactions (green lines) are shown in capped-sticks style with a three-letter code and a sequence number in the protein sequence. Amino acids and ligand atoms are represented by standardized CCDC colors (the gray color represents the **1** carbon core, the red color represents the oxygen atoms, the bluish-purple color represents the nitrogen atom, and the white color represents the hydrogen atoms). The complete amino acid environment in the binding pocket is illustrated in the 2D plots generated using LIGPLUS [71], which are omitted here for clarity.

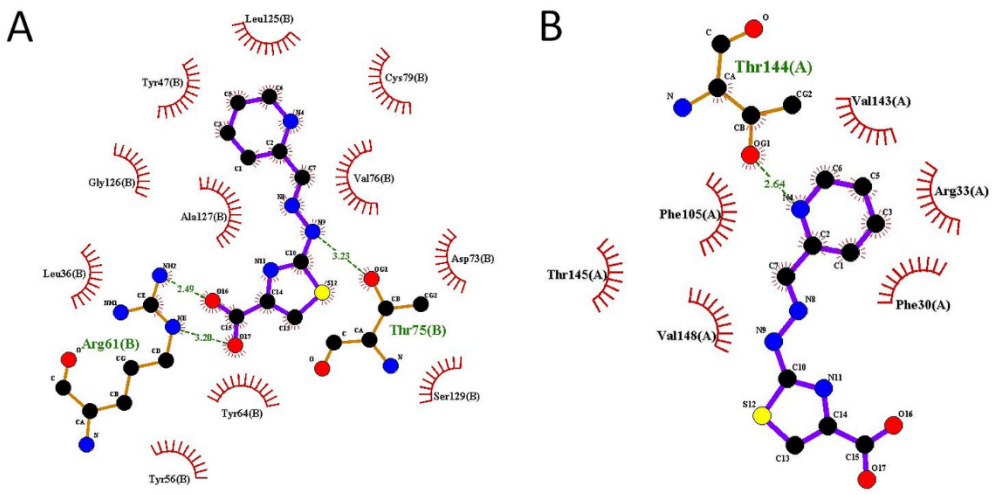


Figure S19. Schematic drawings of the interactions of the first GOLD cluster docked solutions of **monoanionic 1**@LasR transcriptional activator (PDB ID: 3IX3, **A**) and AHL Synthase LasI (PDB ID: 1RO5, **B**)

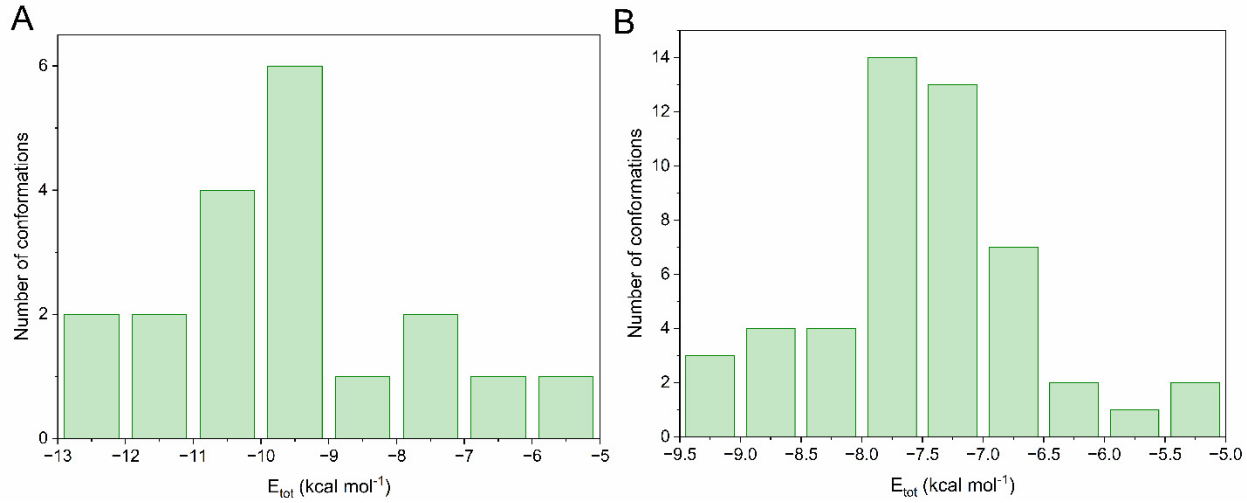


Figure S20. Cluster analysis of docking results of **monoanionic 1**@ LasR transcriptional activator (PDB ID: 3IX3, **A**) and AHL Synthase LasI (PDB ID: 1RO5, **B**) using a 1.0 Å RMSD cluster tolerance.

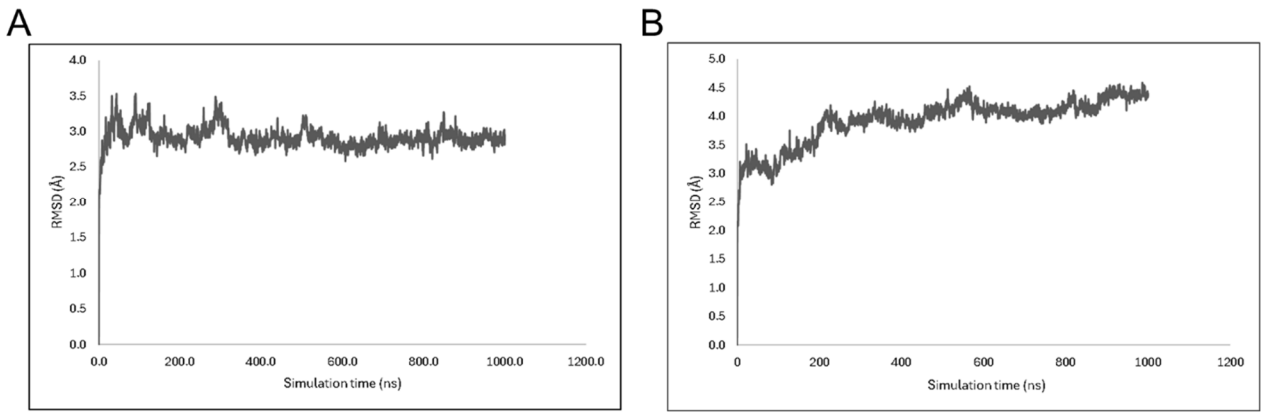


Figure S21. Backbone RMSD trajectories for LasR (A) and LasI (B) proteins–**TTNF37** complexes over the simulation period.of 1000 ns conducted using Desmond software.

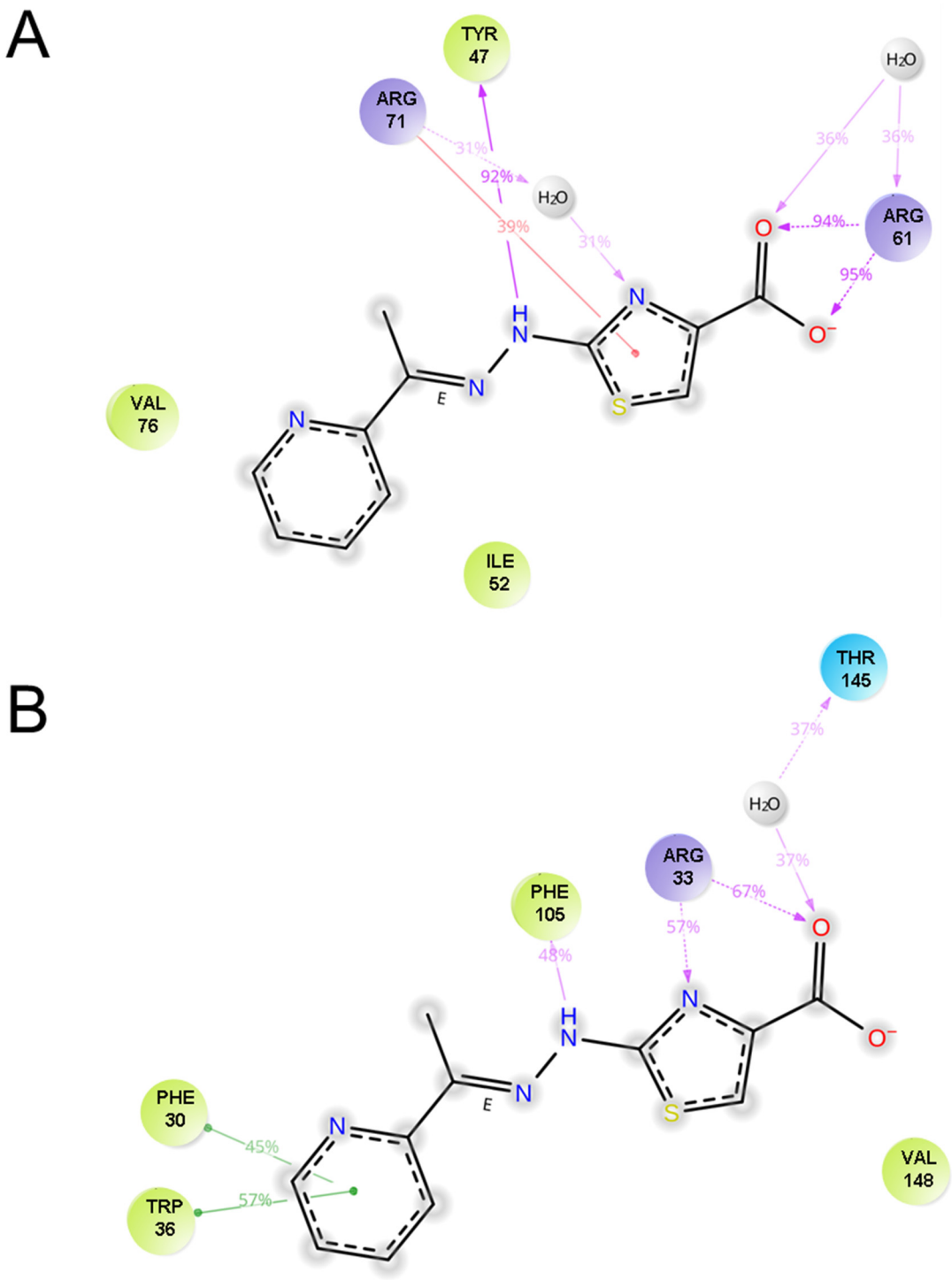


Figure S22. Protein–ligand interaction diagrams from Desmond MD trajectories for LasR (A) and LasI (B) complexes with **TTNF37**, showing hydrogen bonds (purple dashed lines), hydrophobic contacts (green dashed lines), and other key interactions. Percentages indicate the fraction of simulation time each interaction was maintained.